BIOCHEMISTRY
including biophysical chemistry & molecular biology

Article

pubs.acs.org/biochemistry

Solution Structure of the Q41N Variant of Ubiquitin as a Model for the Alternatively Folded N_2 State of Ubiquitin

Soichiro Kitazawa,[†] Tomoshi Kameda,[‡] Maho Yagi-Utsumi,[§,∥] Kenji Sugase,[⊥] Nicola J. Baxter,[#] Koichi Kato,[§,∥] Michael P. Williamson,[#] and Ryo Kitahara*[,†]

[†]College of Pharmaceutical Sciences, Ritsumeikan University, Kusatsu 525-8577, Japan

[‡]Computational Biology Research Center (CBRC), Advanced Industrial Science and Technology (AIST), 2-43 Aomi, Koto, Tokyo 135-0064, Japan

[§]Okazaki Institute for Integrative Bioscience and Institute for Molecular Science, National Institutes of Natural Sciences, Okazaki 444-8787, Japan

[∥]Graduate School of Pharmaceutical Sciences, Nagoya City University, Nagoya 467-8603, Japan

[⊥]Structure and Function Group, Division of Structural Biomolecular Science, Bioorganic Research Institute, Suntory Foundation for Life Sciences, Osaka 618-8503, Japan

[#]Department of Molecular Biology and Biotechnology, University of Sheffield, Firth Court, Western Bank, Sheffield S10 2TN, United Kingdom

Supporting Information

ABSTRACT: It is becoming increasingly clear that proteins transiently populate high-energy excited states as a necessary requirement for function. Here, we demonstrate that rational mutation based on the characteristics of the structure and dynamics of proteins obtained from pressure experiments is a new strategy for amplifying particular fluctuations in proteins. We have previously shown that ubiquitin populates a high-energy conformer, N_2, at high pressures. Here, we show that the Q41N mutation favors N_2: high-pressure nuclear magnetic resonance (NMR) shows that N_2 is ∼70% populated in Q41N but only ∼20% populated in the wild type at ambient pressure. This allows us to characterize the structure of N_2, in which α_1-helix, the following loop, β_3-strand, and β_5-strand change their orientations relative to the remaining regions. Conformational fluctuation on the microsecond time scale, characterized by ^{15}N spin relaxation NMR analysis, is markedly increased for these regions of the mutant. The N_2 conformers produced by high pressure and by the Q41N mutation are quite similar in both structure and dynamics. The conformational change to produce N_2 is proposed to be a novel dynamic feature beyond the known recognition dynamics of the protein. Indeed, it is orthogonal to that seen when proteins containing a ubiquitin-interacting motif bind at the hydrophobic patch of ubiquitin but matches changes seen on binding to the E2 conjugating enzyme. More generally, structural and dynamic effects of hydrodynamic pressure are shown to be useful for characterizing functionally important intermediates.

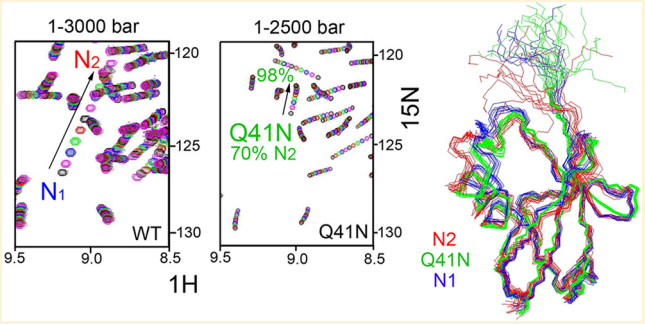

In solution, proteins exist in dynamic equilibrium among multiple conformational states whose Gibbs free energies differ marginally. Conformational fluctuations among different states have long been recognized to be important for protein function, for example, enzyme catalysis.[1−6] Several nuclear magnetic resonance (NMR) approaches that can describe ensembles of high-energy protein conformations in solution have been described. Backbone order parameters obtained from ^{15}N spin relaxation analysis and residual dipolar couplings (RDCs) have been used to describe ensembles of conformations exchanging on time scales of nanoseconds and microseconds, respectively.[7−9] Slower time scale motion, in the range of 100 μs to 10 ms, can be accessed by R_2 relaxation dispersion measurements. Chemical shifts of high-energy conformations obtained from R_2 relaxation dispersion experiments have been used as structural constraints for structure determination.[5,10,11] However, the low populations of such states under physiological conditions continue to make such analyses extremely challenging. In particular, crystal structures of high-energy states are not accessible.

We have shown that high-pressure NMR spectroscopy[12,13] can capture high-energy, typically low-population protein states. In the case of ubiquitin, which plays crucial roles in multiple critical cell functions such as protein degradation in the

Received: October 18, 2012
Revised: February 17, 2013
Published: February 20, 2013

ubiquitin−proteasome system and protein−protein interaction,[14,15] our previous high-pressure NMR investigations[16−21] indicated that ubiquitin exists in equilibrium among the natively folded N_1 state, a totally unfolded U state, and at least two high-energy states: an alternatively folded N_2 state and a less structured I state. Interestingly, we also found that similar high-energy states were conserved in a group of post-translational ubiquitin-like modifiers having the E1−E2−E3 interaction cascade, specifically NEDD8[19] and SUMO-2.[21] The solution structure of ubiquitin at 3 kbar where the N_2 state is 77% populated showed that N_2 has simultaneous reorientation of C-terminal β_5-strand and α_1-helix, providing an open conformation at the C-terminal side of the protein.[18] ^{15}N spin relaxation NMR studies conducted at pressures of up to 3 kbar showed that the conformational fluctuation between N_1 and N_2 occurred in 1−10 μs, with activation volumes of −4 ± 3 and 19 ± 3 mL/mol for N_1 to N_2 and N_2 to N_1 transitions, respectively, at atmospheric pressure. This time scale is too fast to be accessible to R_2 relaxation dispersion experiments.

Interestingly, the pressure-stabilized N_2 structure investigated by solution NMR was reproduced by 1 μs high-pressure molecular dynamics (MD) simulations at 3 and 6 kbar[22] starting from the crystal structure of N_1.[23] These results validate the fact that high-pressure methods can trap high-energy, typically low-population protein states for studies detailing atomic structure. MD simulation revealed that water molecules penetrate the hydrophobic core because of the opening of the C-terminal end of the protein in the N_2 conformer.

Ubiquitin not only is functionally important but also is an important and well-studied target for biophysical investigation. Many studies have investigated its conformational fluctuations,[9,17,18,24−28] but the details of its high-energy states are still not clear. To create mutants that could potentially mimic the solution structure of the N_2 state of the wild-type (WT) protein, we have compared the N_1 (30 bar) and N_2 (3 kbar) structures and found two key structural interactions of the WT protein for controlling N_1−N_2 conformational fluctuations: a hydrogen bond between the I36 backbone carbonyl group and the Q41 side chain amide group and a salt bridge between the K11 amino group and the E34 carboxyl group (Figure 1). Structure and sequence alignments indicated that the hydrogen bond between I36 and Q41 is highly conserved among ubiquitin family proteins, including ubiquitin and NEDD8.[29] Using single-amino acid replacements, we altered the hydrogen bond or salt bridge and created a mutant that favors N_2. This NMR study describes structural, dynamic, and thermodynamic characterizations of the high-energy N_2 state of the protein, which we suggest may be a model for E2 conjugation of ubiquitin.

EXPERIMENTAL PROCEDURES

Sample Preparation. Uniformly ^{15}N-labeled and ^{15}N- and ^{13}C-labeled ubiquitin mutants (K11A, E34A, Q41A, and Q41N) were produced by conventional *Escherichia coli* expression. The protein solution was adjusted to a concentration of 1−2 mM and pH 7.2 at 298 K in 20 mM *d*-Tris-HCl buffer containing 7% ^2H_2O.

The ubiquitin-interacting motif (UIM) of VPS27 was prepared by the F-moc polypeptide synthesis method. The primary structure of the prepared 24-residue peptide was YPEDEEELIRKAIELSLKESRNSA. Residues P2−A24 correspond to residues 256−278 of VPS27. The N-terminal tyrosine is added for a measurement of the peptide concentration by UV absorption.

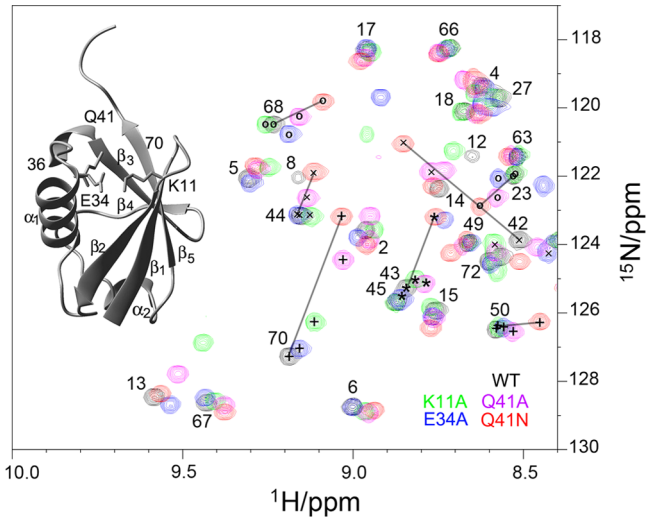

Figure 1. Overlay of the ^{15}N−^{1}H HSQC spectra of WT (black) and mutants of ubiquitin (K11A, green; E34A, blue; Q41A, purple; Q41N, red). The experiments were performed in 1−1.5 mM protein, 20 mM Tris-HCl buffer, and a 7% ^2H_2O/93% H_2O mixture (pH 7.2) at 298 K. Peaks were assigned on the basis of WT spectra using ^{15}N-edited TOCSY and NOESY experiments. The inset shows ubiquitin with the locations of the substituted side chains. Peak positions are indicated for residues 23 (○), 42 (×), 44 (×), 45 (∗) 50 (+), 68 (○), and 70 (+). Lines connect WT (black) and Q41N (red) and show that all mutant peaks lie approximately in a straight line.

NMR Measurements and Analysis. For signal assignments, NMR experiments were performed at 298 K (pH 7.2) on a DRX-600 (^{1}H, 600.23 MHz) spectrometer (BrukerBioSpin Co.). All HSQC cross-peaks in the mutants were assigned to individual amino acid residues using ^{15}N-edited TOCSY and NOESY experiments based on WT assignments. CBCA(CO)NH, HNCACB, HNCA, HN(CO)CA, HNCO, HN(CA)CO, HBHA(CO)NH, CC(CO)NH, HCC(CO)NH, HCCH-TOCY, and CCH-TOCY[30] spectra were recorded on uniformly doubly ^{15}N- and ^{13}C-labeled Q41N ubiquitin. ^{1}H chemical shifts were referenced to the methyl signal of DSS, and ^{15}N and ^{13}C chemical shifts were indirectly referenced to DSS (0 ppm for ^{1}H). Data were processed using Topspin version 1.1 (BrukerBioSpin Co.) and NMRPipe.[31] Signals were assigned using NMRView[32] and KUJIRA.[33]

High-pressure NMR measurements were performed between 1 bar and 3 kbar on WT and Q41N ubiquitin using a DRX500 (^{1}H, 500.13 MHz) spectrometer (BrukerBioSpin Co.) with a capillary pressure-resistance cell[34] or on an AVANCE3-800 (^{1}H, 800.34 MHz) spectrometer (BrukerBioSpin Co.) with a ceramic pressure-resistance cell (Daedalus Innovations).[35]

Structure calculations for the doubly ^{15}N- and ^{13}C-labeled Q41N ubiquitin were performed with CYANA version 3.93[36] with distance and angle constraints. Distance constraints were obtained from ^{15}N-edited NOESY, ^{13}C-edited NOESY, and ^{13}C-edited aromatic NOESY spectra with a mixing time of 100 ms. The backbone ϕ angle constraints were derived from J coupling constants based on ^{15}N-edited HNHA[37] measurements with the following criteria: $-160° < \phi < -80°$ for $J > 8$ Hz, and $-90° < \phi < -40°$ for $J < 6$ Hz. Backbone ϕ and φ angle constraints were also derived using TALOS$^+$:[38] for β-sheet, $-120° < \phi < -20°$ and $-100° < \phi < 0°$, and for α-helix,

dx.doi.org/10.1021/bi301420m | *Biochemistry* 2013, 52, 1874−1885

$-200° < \phi < -80°$ and $40° < \phi < 220°$. $^{1}H-^{15}N$ residual dipolar couplings (RDCs) were used for angle constraints with a 0.5 Hz error. The weight of the RDC constraints[39] in the CYANA calculation was set to 0.05 (5%). For structure refinement, energy minimization was performed in explicit water (TIP3P) with distance and angle constraints using AMBER11.[40]

^{15}N relaxation parameters, R_1, R_2, and $^{15}N-^{1}H$ heteronuclear NOE, were obtained at 278 and 298 K using a DRX-600 spectrometer with pulse sequences described in the literature.[41] In addition, ^{15}N-R_2 was obtained using an AVANCE3-950 (^{1}H, 950.33 MHz) spectrometer (BrukerBioSpin Co.). Model-free analysis was performed using Modelfree version 4.15[42] and its interface program FAST-Modelfree[43] under the assumption of axially symmetric molecular tumbling. The $^{15}N-^{1}H$ internuclear distance and the ^{15}N chemical shift anisotropy were assumed to be 1.02 Å and −170 ppm, respectively.

Relaxation dispersion measurements were conducted on an AVANCE3-800 (^{1}H, 800.34 MHz) spectrometer under high pressure as described previously[44] using a ceramic high-pressure cell.

Phase-modulated clean chemical exchange (CLEANEX-PM) fastHSQC NMR experiments[45] were performed at 298 K (pH 7.2 and 7.6) using a DRX-600 spectrometer with six mixing times (0.005, 0.010, 0.015, 0.02, 0.05, and 0.1 s), where magnetization is transferred from solvent water to amide hydrogens of the protein. Spectra were collected with an increment delay of 2 s. As a reference, fastHSQC without the mixing times was collected. The water−amide hydrogen exchange rate is estimated by the following equation.

$$I/I_0 = k/(R_{1A} + k - R_{1B}) \times \{\exp(-R_{1B}\tau_m) - \exp[-\tau_m(R_{1A} + k)]\} \quad (1)$$

where k is the normalized rate constant related to the pseudo-first-order, forward rate constant $k_{BA}(H_2O \rightarrow NH) = X_B k$, X_B is the mole fraction of water (approximately 1), R_{1A} is a combination of longitudinal and transverse relaxation rates in the CLEANEX measurement, and R_{1B} is the longitudinal relaxation rate for water (0.6 s^{-1} was used in this experiment).[45] I is the peak intensity in the spectrum at different mixing time τ_m, and I_0 is that in a reference spectrum.

Determination of K_d Values from NMR Titration Curve Fitting. The 1:1 binding model was used for the fitting of the ^{15}N chemical shift changes ($\Delta\delta$) observed in the titration of ubiquitin with UIM. Assuming that the observed $\Delta\delta$ is a weighted average between two extreme values corresponding to the free and UIM-bound states, we use the following equation for our analysis

$$P_b = \{1 + M + A - [(1 + M + A)^2 - 4M]^{0.5}\}/2 \quad (2)$$

where P_b is the population of ubiquitin bound to UIM, $M = [UIM]/[Ub]$, and $A = K_d/[Ub]_{total}$. Details of the analysis are discussed in the literature.[34] The K_d values are obtained by a global fit.

Thermodynamic Analysis. For the case in which the two conformers, N_1 and N_2, are in rapid exchange on the NMR time scale, the observed chemical shift δ is related to the equilibrium constant K_{obs} by eq 3:

$$K_{obs} = (\delta_{N_1} - \delta)/(\delta - \delta_{N_2}) \quad (3)$$

where δ_{N_1} and δ_{N_2} are the intrinsic chemical shifts of conformers N_1 and N_2, respectively, and δ is the observed chemical shift at a given pressure. Assuming no compressibility change with pressure, the Gibbs free energy difference between N_1 and N_2 is expressed by eq 4:

$$\Delta G_p = -RT \ln K_{obs} = \Delta G° + \Delta V°(p - p°) \quad (4)$$

where R is the gas constant and ΔG_p and $\Delta G°$ are the Gibbs free energy differences at pressure p and 1 bar, respectively. $\Delta V°$ is the partial molar volume difference between N_1 and N_2 at 1 bar. By combining eqs 3 and 4, we can express the chemical shift by eq 5

$$\delta = \frac{\delta_{N_1} + \delta_{N_2} \exp\left[-\frac{\Delta G° + \Delta V°(p - p°)}{RT}\right]}{1 + \exp\left[-\frac{\Delta G° + \Delta V°(p - p°)}{RT}\right]} \quad (5)$$

Chemical shifts at different pressures were fit to eq 5 with four variables: δ_{N_1}, δ_{N_2}, $\Delta G°$, and $\Delta V°$. We performed a global fitting for multiple ^{1}H and ^{15}N chemical shift data of different residues. For the WT sample, $\Delta G°$ and $\Delta V°$ are global variables. For Q41N, $\Delta G°$ is a global variable but $\Delta V°$ is assumed to be the same as that of WT.

RESULTS

Figure 1 shows a superposition of the $^{15}N-^{1}H$ HSQC spectra of uniformly ^{15}N-labeled wild-type ubiquitin and four different mutants: K11A, E34A, Q41A, and Q41N. Several peaks in segments 30−45 and 68−73 show substantial changes in ^{15}N and ^{1}H chemical shifts upon mutation. Interestingly, for many residues, the chemical shift changes in the different mutants fall close to a straight line, and the magnitudes of the shift changes are consistently in the following order: K11A ≈ E34A < Q41A < Q41N [with the exception of residues located near the mutation sites (Figure 1)]. A more detailed analysis shows that the pattern of shift changes from the mutations is strongly correlated, particularly in α_1-helix, the following loop, β_3-strand, and β_5-strand (Figure S1 of the Supporting Information). Because an NMR chemical shift is a population-weighted average among conformers exchanging on a time scale faster than the NMR time scale, these correlated changes in chemical shifts indicate that the mutations all have a similar effect on the structure, namely, to move the population from the native folded N_1 state to the same high-energy state of the protein. The order of shift changes of the mutants shows how fully this conformational change has occurred.

Previously, we have shown that an increase in pressure from 30 bar to 3.5 kbar at 293 K causes changes in chemical shifts in ubiquitin that can be fit well to a transition between two conformations, N_1 and N_2.[16] A comparison of these chemical shift changes with those resulting from the Q41N mutation shows a significant correlation (Figure S2 of the Supporting Information), especially noteworthy considering that hydrostatic pressure also affects chemical shifts by compression of covalent bonds[46] and heterogeneous compression within the protein.[47] Therefore, we may conclude that the population of the N_2 state of the protein is increased through these mutations, as it is by high pressure.[16,18]

To estimate the population of N_2 in WT and Q41N, high-pressure NMR experiments were conducted for WT and Q41N under the same conditions (pH 7.2, 298 K, and same buffer). Panels A and B of Figure 2 show a superposition of HSQC

dx.doi.org/10.1021/bi301420m | Biochemistry 2013, 52, 1874−1885

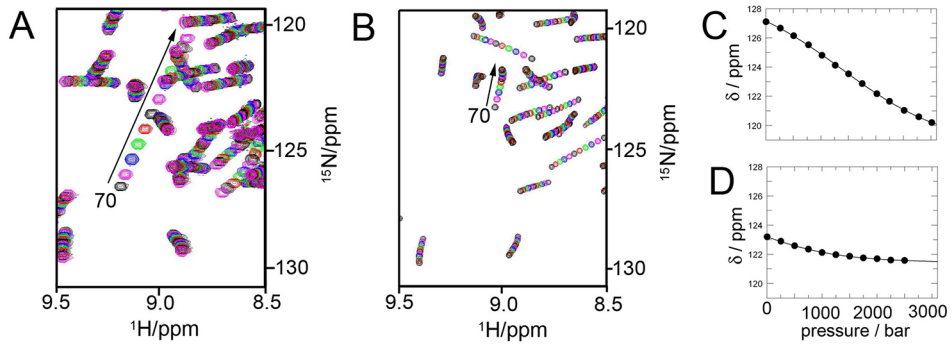

Figure 2. (A and B) Superposition of HSQC spectra of (A) WT and (B) Q41N ubiquitin at different pressures. High-pressure experiments were performed up to 3 kbar for WT on a ^{1}H 500 MHz spectrometer and up to 2.5 kbar for Q41N on a ^{1}H 800 MHz spectrometer. The pressure-induced shift of the cross-peak for V70 is marked with an arrow. (C and D) Pressure-induced ^{15}N chemical shifts of V70 for (C) WT and (D) Q41N.

spectra of WT and Q41N, respectively, at different pressures. Sigmoid-shaped changes were obtained for ^{1}H and ^{15}N chemical shifts of some residues of the WT protein with pressure (e.g., residues 7, 8, 33, 42, and 70). Figure 2C shows representative pressure-induced ^{15}N chemical shifts of WT V70. Assuming two-state exchange between N_1 and N_2, a global fitting was performed for the WT protein (see Experimental Procedures). Seven chemical shift data sets (^{1}H shifts of residues 7, 8, 33, 42, and 70 and ^{15}N shifts of residues 42 and 70) were used for the fitting with four variables for each data set (Figure 3): N_1 and N_2 chemical shifts, the Gibbs free energy difference $\Delta G°$, and the partial molar volume difference $\Delta V°$ between N_1 and N_2. As a result of the fitting, the global parameters $\Delta G°$ and $\Delta V°$ for WT at pH 7.2 were estimated to be 3.4 ± 0.13 kJ/mol and −24.7 ± 0.8 mL/mol, respectively

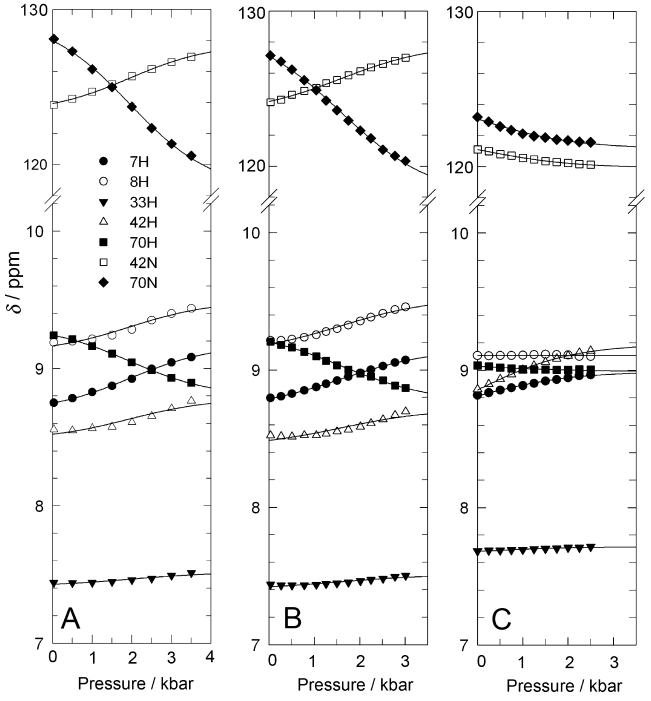

Figure 3. Plots of ^{15}N and ^{1}H chemical shifts of amide groups of selected residues (7, 8, 33, 42, and 70) as a function of pressure. (A) WT ubiquitin at pH 4.7 and 20 °C.[16] (B) WT ubiquitin at pH 7.2 and 25 °C. (C) Q41N ubiquitin at pH 7.2 and 25 °C. These curves are the fits obtained by global fitting of the shifts (see Experimental Procedures).

(Figure 3B and Table 1), which are comparable to those previously measured for WT protein at pH 4.7 (3.9 kJ/mol and

Table 1. Thermodynamic Parameters for the Transition from N_1 to N_2 and Limiting Chemical Shifts (^{1}H or ^{15}N, in parts per million) of Selected Residues

		WT (pH 4.7, 293 K)	error	WT (pH 7.2, 298 K)	error	Q41N (pH 7.2, 298 K)	error
$\Delta G°$ (kJ/mol)		3.9	0.16	3.4	0.13	−2.2	0.3
$\Delta V°$ (mL/mol)		−22.7	0.9	−24.7	0.8	−24.7	−[a]
7H	δ_{N_1}	8.65	0.03	8.70	0.019	8.40	0.07
	δ_{N_2}	9.16	0.03	9.13	0.018	8.97	0.01
8H	δ_{N_1}	9.09	0.03	9.10	0.02	9.10	0.05
	δ_{N_2}	9.48	0.02	9.50	0.018	9.11	0.01
33H	δ_{N_1}	7.41	0.02	7.40	0.019	7.60	0.05
	δ_{N_2}	7.51	0.02	7.51	0.017	7.71	0.01
42H	δ_{N_1}	8.47	0.03	8.42	0.019	8.07	0.10
	δ_{N_2}	8.77	0.02	8.78	0.017	9.16	0.01
70H	δ_{N_1}	9.34	0.03	9.32	0.02	9.12	0.05
	δ_{N_2}	8.81	0.03	8.79	0.018	8.90	0.01
42N	δ_{N_1}	123.09	0.08	123.23	0.07	123.9	0.3
	δ_{N_2}	127.69	0.07	127.68	0.06	120.03	0.01
70N	δ_{N_1}	130.12	0.17	129.42	0.16	127.7	0.5
	δ_{N_2}	118.69	0.16	118.52	0.13	121.34	0.015

[a]For the analysis of Q41N, the ΔV value of WT at pH 7.2 (−24.7 mL/mol) is used, as a constant.

−22.7 mL/mol, respectively). These values imply that the population of N_2 in the WT protein is ∼20% at 1 bar and 80% at 3 kbar. In contrast, the pressure-dependent chemical shifts in Q41N suggest that even at 1 bar it is predominantly N_2. As a representative, ^{15}N chemical shifts of V70 for Q41N are shown in Figure 2D. This makes it more difficult to fit the shifts accurately, because much less of the transition is experimentally accessible. Consequently, $\Delta V°$ for Q41N was assumed to be the same as that of WT (i.e., −24.7 mL/mol). $\Delta G°$ was then fit to be −2.2 ± 0.3 kJ/mol, showing a population of N_2 of 71% at 1 bar and 98% at 3 kbar. Thermodynamic parameters for WT and Q41N proteins obtained by the fittings are summarized in Table 1.

dx.doi.org/10.1021/bi301420m | Biochemistry 2013, 52, 1874−1885

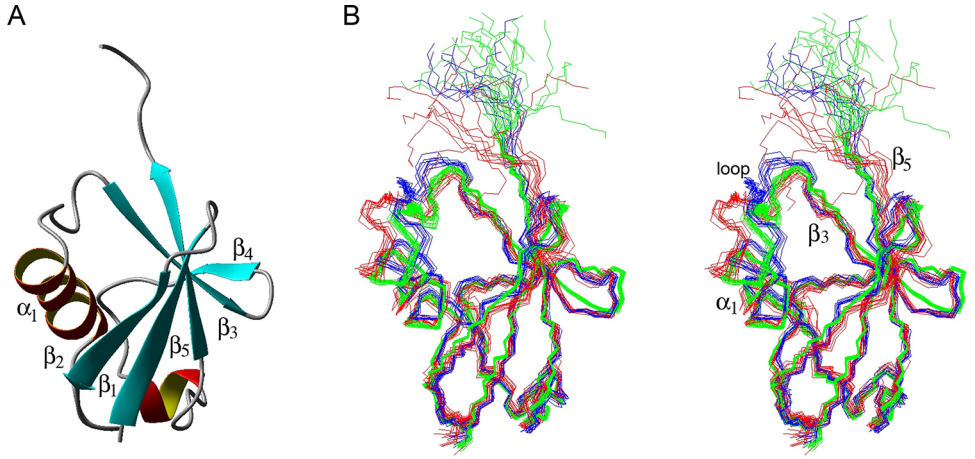

Figure 4. Solution structure of Q41N ubiquitin, the first model mutant of the N_2 conformation of ubiquitin. (A) Ribbon representation of the lowest-energy model. (B) Stereoviews of the 20 lowest-energy structures of Q41N (green, PDB entry 2RSU), the 10 lowest-energy structures of N_1 at 30 bar (blue, PDB entry 1V80), and the 10 lowest-energy structures of N_2 at 3 kbar (red, PDB entry 1V81) of the WT protein. The ubiquitin structures at 30 bar and 3 kbar were also energy-minimized the same way. All models are calculated with CYANA (version 1.2 for WT or version 3.93 for Q41N) and energy-minimized using AMBER11. Large displacements from N_1 (blue) are observed at α_1-helix, the following loop, β_3-strand, and β_5-strand.

To further understand the structural changes that occur because of the Q41N mutation, we determined the solution structure of the mutant using distance and angle constraints. Distance constraints were obtained from ^{15}N-edited NOESY, ^{13}C-edited NOESY, and ^{13}C-edited aromatic NOESY with a 100 ms mixing time. The backbone ϕ and φ angle constraints were derived from J coupling constants (^{15}N-edited HNHA) and chemical shifts (^{1}H, ^{15}N, and ^{13}C) using TALOS^{+}.[38] Angle constraints for backbone NH groups were obtained by ^{1}H−^{15}N residual dipolar couplings (RDCs).[39] Structures were calculated using CYANA version 3.93[36] and then energy-minimized using AMBER11[40] in explicit water (TIP3P). Figure 4A shows a ribbon model of the refined structure, and geometrical statistics are summarized in Table 2. Because Q41N has a 71:29 ratio of N_2 to N_1, the averaged structures derived by this NMR analysis do not fully represent 100% N_2. However, given the r^{-6} dependence of NOEs and the network anchoring algorithm of CYANA,[36] which are both likely to reduce the impact of NOEs from the N_1 minor conformer, the structure is likely to be heavily biased toward the pure N_2 conformer. Stereopairs of the 20 lowest-energy structures of Q41N (green) are compared with WT N_1 at 30 bar (blue) and N_2 at 3 kbar (red) (Figure 4B). The resultant structure of the mutant reveals a large displacement of α_1-helix, the following loop, and C-terminal β_5-strand compared to those of N_1, while the hydrophobic patch centered on I44 in the β-sheet region is almost intact. Chemical shift differences in amide H, amide N, C′, Cα, and Hα were also analyzed to evaluate the obtained structure (Figure S3 of the Supporting Information). Large differences were observed at several residues along α_1-helix, the following loop, β_3-strand, and β_5-strand. In particular, changes are substantial at residues 27, 30, 70, and 71, these being the largest changes in the protein except for that of residue 41 that is substituted in the mutant. Because the amide N, C′, Cα, and Hα chemical shifts are sensitive to the backbone torsion angles ϕ and φ, the large changes in chemical shifts coincide well with the changes in the backbone orientations of these residues. We calculated the chemical shifts of the Q41N structure by using SHIFTX2 version 1.07.[48] There are highly significant correlations between observed (raw values) and back-calculated chemical shifts (R

Table 2. Statistics of 20 NMR Structures of Q41N Mutant Ubiquitin at 1 bar and 298 K[a]

restraints used in the structure calculation	
no. of distance constraints	1455
no. of ϕ angle constraints[b]	36
no. of ϕ and φ angle constraints[c]	80
no. of angle constraints from residual dipolar couplings[d]	67
residual violations in the CYANA calculation	
target function values (Å^2)	3.99 ± 0.04
no. of van der Waals restraint violations[e]	3
no. of residual dipolar coupling restraint violations[e]	3
residual violations after AMBER energy minimization	
close contacts	1
distance deviation of >0.2 Å (no. of violations)	0.23 ± 0.02 (2)
RDC deviation (Hz)	0.74 ± 0.33
geometric statistics[f]	
average backbone atom rmsd from the mean (Å)	0.21
average heavy atom rmsd from the mean (Å)	0.65
Ramachandran analysis[g]	
most favored regions (%)	87.5
additional allowed regions (%)	12.5
disallowed regions (%)	0.0

[a]Twenty structures with the lowest target function are selected from 200 structures calculated with CYANA version 3.93 from randomized starting structures. Atomic coordinates and structure constraints are deposited as PDB entry 2RSU. Signal assignments are deposited as BMRB entry 11505. [b]Torsion angle constraints obtained from J coupling constants by a three-dimensional HNHA experiment: $-160° < \phi < -80°$ for $J > 8$ Hz, and $-90° < \phi < -40°$ for $J < 6$ Hz. [c]Torsion angle constraints from chemicals shifts using TALOS^{+}: for β-sheet, $-120° < \phi < -20°$ and $-100° < \phi < 0°$, and for α-helix, $-200° < \phi < -80°$ and $40° < \phi < 220°$. [d]^{1}H−^{15}N residual dipolar couplings are used for the angle constraints with a 0.5 Hz error. The weight of the RDC constraints in the CYANA calculation is set to 0.05. [e]Constraints violated in more than six structures. [f]rmsd for residues 1−70. [g]Ramachandran analysis for residues 1−74. Pro and Gly are not involved in the evaluation.

dx.doi.org/10.1021/bi301420m | Biochemistry 2013, 52, 1874−1885

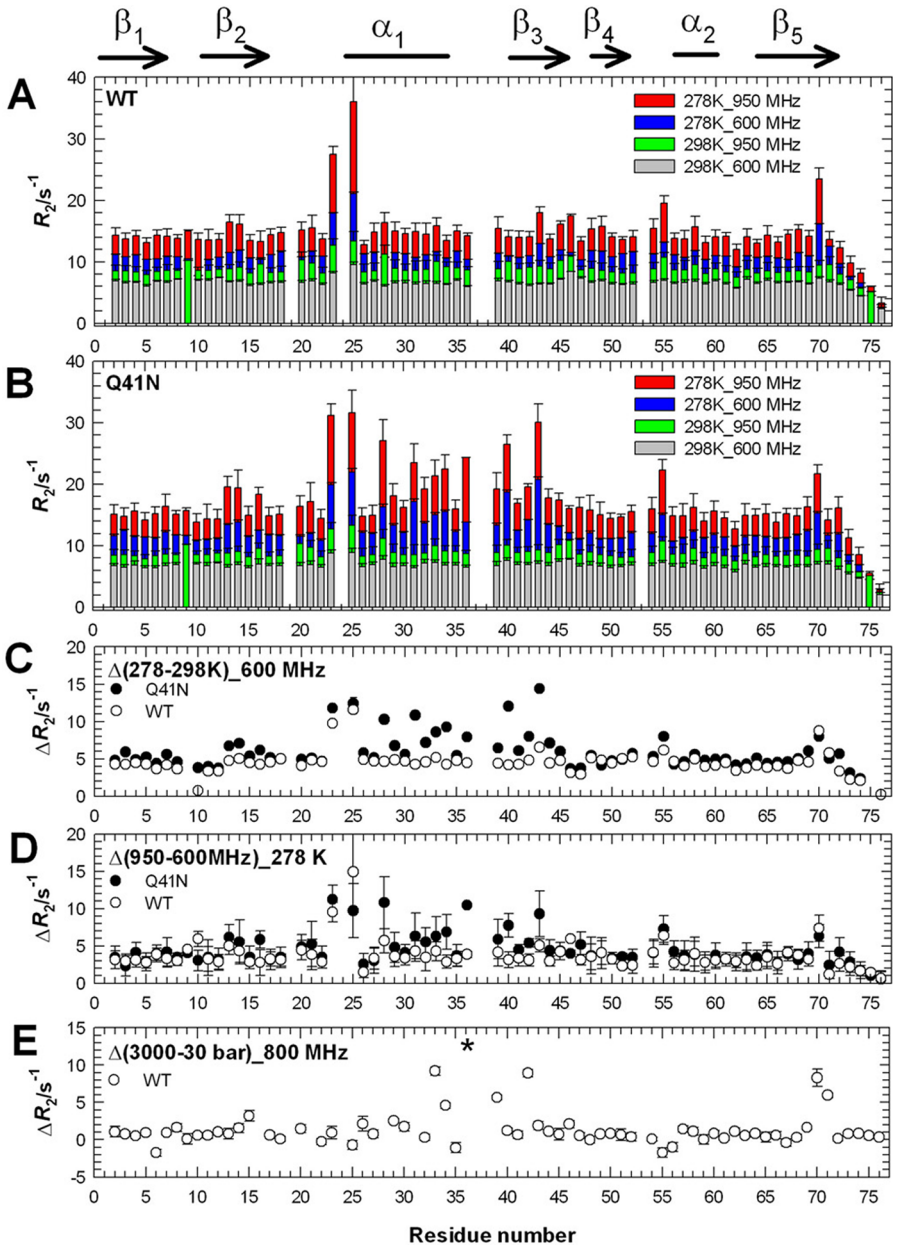

Figure 5. ^{15}N transverse relaxation rates, ^{15}N-R_2, of (A) WT and (B) Q41N ubiquitin. ^{15}N transverse relaxation NMR experiments were performed at ^{1}H 600.23 MHz (298 K, gray; 278 K, blue) and ^{1}H 950.33 MHz (298 K, green; 278 K, red) frequencies. R_2 experiments were performed with 10 relaxation delays from 20 to 280 ms (600 MHz) and seven relaxation delays from 20 to 150 ms (950 MHz). Residues 19, 37, and 38 are prolines, giving no data. Severe line broadening prohibited quantitative evaluation of R_2 values for residues 24 and 53 under all experimental conditions. (C) Difference of ^{15}N-R_2 between 278 and 298 K (^{1}H, 600 MHz) for WT (○) and Q41N (●). (D) Frequency dependence (950 to 600 MHz) of ^{15}N-R_2 at 278 K for WT (○) and Q41N (●). (E) Effects of pressure on ^{15}N-R_2 of the WT protein at 293 K. Data were collected on a ^{1}H 800 MHz spectrometer.[18] The asterisk indicates residue 36, for which data were not available because of severe line broadening. Secondary structures are indicated at the top of the panel.

values of 0.90 for amide H, 0.91 for amide N, 0.87 for C′, 0.99 for Cα, 0.94 for Hα, and >0.99 for C$_\beta$), which validate the backbone orientations of Q41N determined by NMR. These structural characteristics are very similar to those of N_2 stabilized at 3 kbar, although the orientations of the α_1-helices do not exactly match. However, these structural features confirm that the alternatively folded structures produced by pressure and by the Q41N mutation are essentially identical. To evaluate how well the RDCs of Q41N fit to the N_1 and N_2 conformations, RDC values were back-calculated from the structures of WT at 30 bar (N_1 model) and 3 kbar (N_2 model) and compared to the RDCs of Q41N. The difference between experimental and back-calculated RDCs for residues 23−43 is larger for WT at 30 bar (average of 4.1 Hz) than for WT at 3 kbar (average of 2.5 Hz). These results confirm that N_2 is a better model for Q41N than N_1.

Changes in dynamics of the protein are manifested by ^{15}N spin relaxation NMR spectroscopy. Figure 5 shows the ^{15}N transverse relaxation rate constants R_2[41] of the backbone amide groups for WT (A) and Q41N (B), which are sensitive probes of the microsecond to millisecond motion of proteins. R_2 values were collected at two different temperatures, 298 and 278 K,

dx.doi.org/10.1021/bi301420m | *Biochemistry* 2013, 52, 1874−1885

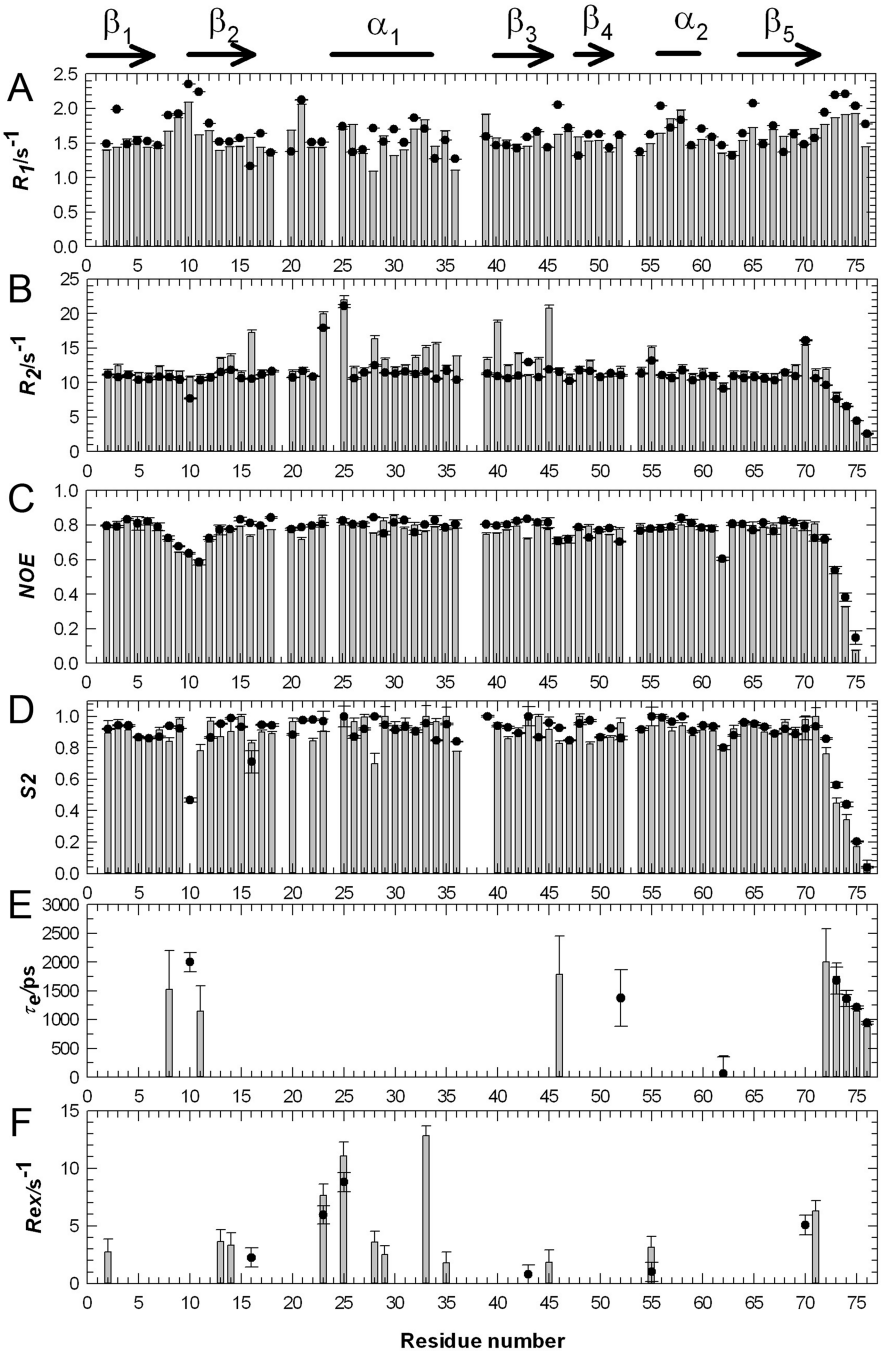

Figure 6. ^{15}N spin relaxation dynamics of ubiquitin mutant Q41N (histograms) and WT (●) at pH 7.2 and 278 K. The data were collected at a ^{1}H frequency of 600.23 MHz and a ^{15}N frequency of 60.83 MHz. (A) ^{15}N longitudinal relaxation rates, R_1. (B) ^{15}N transverse relaxation rates, R_2. (C) Heteronuclear Overhauser effects, ^{15}N-NOE. (D) Order parameters of NH vectors, S^2. (E) Internal correlation times, τ_e. (F) Exchange contributions to ^{15}N transverse relaxation rates, R_{ex}. Plots in panels D−F were obtained from a model-free analysis of the spin relaxation parameters for the protein with ModelFree version 4.15 and its interface program FAST-Modelfree assuming axially symmetric molecular tumbling. The overall rotational correlation time was set to 8.1 ns for both Q41N and WT proteins. Relaxation parameters are deposited as BMRB entry 11505.

and at ^{1}H 600 MHz and ^{1}H 950 MHz frequencies. For WT and Q41N at 298 K, the R_2 values are almost constant along the sequence, except for those of the residues in the flexible C-terminal region. Unlike in WT, in Q41N, the R_2 values for the α_1-helix, the following loop, and β_3-strand at 278 K and 600 MHz are approximately 10 s^{-1} larger than those of the WT protein (Figure 5B,C). To characterize these dynamics in greater detail, we conducted the model-free analysis of Lipari and Szabo[49,50] using ^{15}N-R_1, R_2, and NOE data collected at 278 K (Figure 6). The order parameters S^2, which represent the degree of spatial restriction of individual N−H vectors on the picosecond to nanosecond time scale, are nearly equivalent between WT and Q41N, except for a substantial decrease in the S^2 of residue 28 at the center of α_1-helix. Assuming the simplest model for fast conelike motions of the NH vector, a decrease in S^2 (e.g., 1.0 → 0.7) for the NH vector of residue 28 implies an increase in the amplitude of the motion (e.g., 0° → 30°) at the center of α_1-helix in Q41N.[49] These dynamic characteristics on

dx.doi.org/10.1021/bi301420m | Biochemistry 2013, 52, 1874−1885

the picosecond to nanosecond time scale at the center of α_1-helix could be the origin of the structural differences seen in this region (Figure 4B). This idea is consistent with that seen by chemical shift changes (Figure S3 of the Supporting Information). In contrast, the conformational exchange contribution R_{ex} to the transverse relaxation constant, namely a conformational fluctuation taking place on the microsecond to millisecond timescale, is significantly increased in Q41N compared to that in WT at 278 K, especially at residues 13, 14, 23, 25, 28, 29, 33, and 71. In addition, substantial increases in R_2 are observed for several residues in α_1-helix, the following loop, β_3-strand, and β_5-strand at 950 MHz and 278 K (Figure 5D). The static magnetic field dependence of R_2 also indicates the presence of an exchange contribution to R_2 in these regions of Q41N. These regions coincide well with those showing large structural displacements in the mutant protein. Indeed, there is a significant correlation between changes in ^{15}N-R_2 and δ^{15}_N on mutation (R = 0.35 for 67 R_2 data). It is noteworthy that similar increases (approximately 12 s^{-1}) in R_{ex} were observed for these regions of the WT protein at 3 kbar (293 K) (Figure 5E), where the N_2 conformer forms 77% of the solution population and the exchange rate constants (k_{12} + k_{21}) are ~3 times smaller (k_{12} = 1.27 × 10^5 s^{-1} and k_{21} = 0.38 × 10^5 s^{-1} at 3 kbar and 293 K) than those typically found at 1 bar.[18] The similarity between effects of mutation and pressure on R_2 (R = 0.69 for 67 R_2 data) strongly indicates that the R_{ex} observed for Q41N at 278 K originates primarily from the fluctuation between conformers N_1 and N_2. The exchange contribution is enhanced in the mutant sample due, most likely, to a further increase in the N_2 population and a slowing of the exchange rate constants (k_{12} + k_{21}) at low temperatures, similar to the WT protein under high pressure. Relaxation dispersion experiments have been conducted with WT and Q41N at a range of pressures and confirm these observations, further suggesting that exchange remains faster than approximately 10^4 s^{-1} even at 278 K and 2 kbar (Figure S4 of the Supporting Information).

To further characterize the dynamics and stability of the protein, we performed CLEANEX-PM NMR experiments[45] at pH 7.2 for the WT and Q41N proteins. CLEANEX-PM spectra are shown in Figure S5 of the Supporting Information, and an analysis of the water–amide proton exchange rates with the assumption of a pseudo-first-order reaction is shown in Figure 7. The WT protein demonstrated exchange rates faster than 0.01 s^{-1} for exposed backbone amide protons that were hydrogen-bonded with water molecules and were therefore actively exchanging (Figure 7A,C). In contrast, remarkable increases in water–amide proton exchange rates were observed at residues 31–33, 35, 40, and 41 at the end of α_1-helix, the following loop, and the beginning of β_3-strand in Q41N (Figure 7B,D). Because many of these residues are involved in the conformational transition from N_1 to N_2,[18] these increases in water–amide proton exchange rates can be explained by the swinging out of α_1-helix with a simultaneous reorientation of C-terminal β_5-strand and concomitant penetration of water into the hydrophobic cavity, as predicted by high-pressure NMR[18] and MD simulation[22] for the WT protein. Similar but smaller changes in water–amide proton exchange rates are observed for similar regions in Q41A, but they are much smaller in K11A and E34A (Figure S6 of the Supporting Information), suggesting that the observed increase in the water–amide proton exchange rates of α_1-helix and loop regions in the ubiquitin mutants can be attributed to an increased N_2 population that is preferentially favored, especially in the Q41N mutant as compared to the WT.

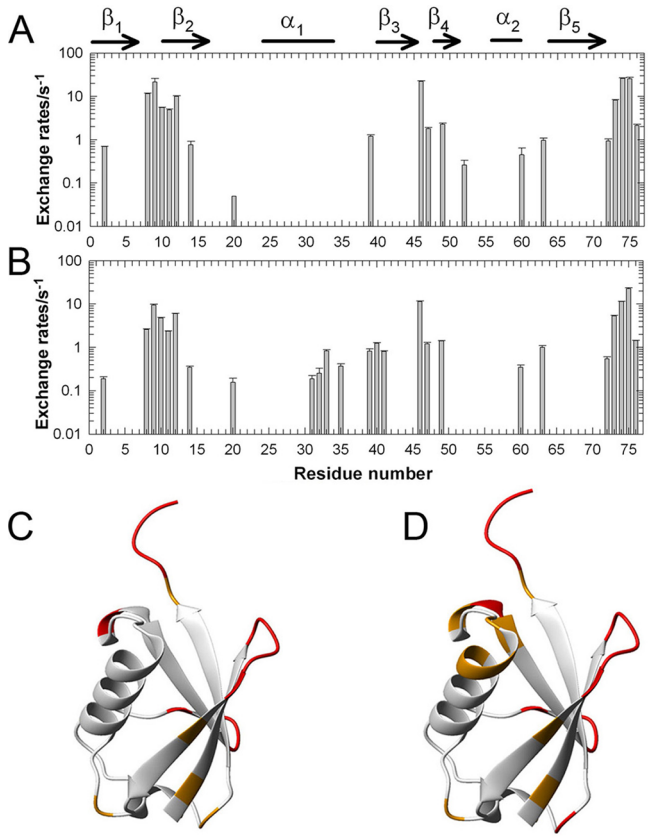

Figure 7. Comparison of water–amide proton exchange rates for ubiquitin in (A and C) WT and (B and D) Q41N. The water–amide proton exchange rates are estimated by a least-squares fitting assuming a pseudo-first-order reaction (H_2O → NH). For Q41N, the water–amide proton exchange rates are obtained at pH 7.2 (histogram). The residues that show faster water–amide proton exchanges are marked by colors according to their rate constants (k): k > 1 s^{-1} (red), and 1 s^{-1} > k > 0.01 s^{-1} (orange).

To understand the functional importance of the N_2 state of ubiquitin, we examined the association between the ubiquitin-interacting motif (UIM) of Vps27 and ubiquitin (UB) for both WT and Q41N mutant samples. The UIM is found in many trafficking proteins; in particular, the Vps27 UIM is involved in the pathways of endocytosis and vacuolar protein sorting.[51] Nine HSQC measurements were taken at [UIM]/[UB] ratios varying from 0 to 3.4. According to the solution structure of the ubiquitin–UIM complex,[51] the UIM binds to the β-sheet region that comprises β_1-, β_3-, and β_5-strands (Figure 1) and the hydrophobic patch centered on I44, which is a binding region for many interacting proteins.[29] ^{15}N chemical shifts of several residues located on these β-strands were used in a two-state binding model analysis (Figure S7 of the Supporting Information). The dissociation constant K_d for UIM is estimated from 13 data sets (residues 7, 11, 13, 41, 43, 44, 46–48, and 69–72) as 230 ± 30 μM for Q41N, which is identical within error to that for WT (210 ± 11 μM). These results indicate that the N_1–N_2 fluctuation has little effect on binding with the UIM. Furthermore, the changes in ^{1}H and ^{15}N chemical shifts induced by mutation observed in free ubiquitin are retained in the UIM complex, except in some of the β_3- and β_4-strands where the UIM binds (Figure S8 of the Supporting

dx.doi.org/10.1021/bi301420m | Biochemistry 2013, 52, 1874–1885

Information). This means that the N_2 state continues to be significantly populated, even in the UIM-bound form of the mutant sample.

DISCUSSION

Pressure and Mutation Effects. Here, we have shown that four mutations in ubiquitin produce highly correlated sets of chemical shift changes, and that these chemical shift changes also correlate with shift changes caused by pressure perturbation. The shift changes are spatially grouped together in α_1-helix, the following loop, β_3-strand, and β_5-strand. NMR relaxation experiments show changes in dynamics in the same residues, again with parallel effects in the mutants and at high pressure. These results indicate that mutation and pressure mainly act to shift the population from the native N_1 conformation to a higher-free energy N_2 conformation. For Q41N, the N_1:N_2 population ratio is 29:71 at atmospheric pressure.

The correlation between mutation and pressure effects can be explained by the Gibbs free energy difference (ΔG) between any two conformers (eq 4). The structure of a protein is closely coupled to its partial molar volume, and typically as it unfolds under physiological conditions, there is a corresponding decrease in the partial molar volume due to the hydration of its internal cavities and solvent contraction around the hydrated charge groups. Thus, in general, pressure can cause a population shift among protein conformers through the $\Delta V^\circ(p - p^\circ)$ relationship of eq 4. This population shift occurs with the highest-molar volume conformer, N_1, which has the lowest Gibbs free energy and is the most stable and ordered, through to the various lower-volume conformers, N_2 and I, that have a less ordered conformation, and finally to the lowest-volume conformer, U, which has the highest energy and is unstable and disordered.[17]

In contrast, mutant ubiquitin at constant temperature and pressure will undergo a change in ΔG° (eq 4) upon a transition in conformation that results from changes in ΔH° and ΔS° ($\Delta G^\circ = \Delta H^\circ - T\Delta S^\circ$). The structure obtained by NMR shows that the Q41 → N mutation weakens the interaction between the loop and β_3-strand by the loss of the hydrogen bond between the I36 C═O group and the Q41 side chain NH_2 group. Moreover, the mutation causes significant amplification of the microsecond to millisecond time scale motion and hydration at the backbone sites of α_1-helix, the following loop, β_3-strand, and β_5-strand (see Water−Amide Proton Exchange and Thermodynamic Stability). These enthalpic and entropic effects on mutation are considered to be the reasons for the increase in the population of the N_2 conformer in the Q41N sample.

The changes in structure and dynamics (e.g., atomic coordinates, chemical shifts, and ^{15}N-R_2 values) show a similar tendency, but do not exactly match, between mutation and pressure perturbations. Although neither the Q41N structure at 1 bar nor the wild-type structure at 3 kbar is 100% N_2, the similarities in their features suggest that the wild-type N_2 state at 1 bar is closely similar to both. The discrepancy can be explained by the other effects of mutation and pressure. For instance, mutation changes the atomic packing around the nuclei that are spatially close to the substituted side chain, while increased pressure reduces the entire structural volume, namely atomic packing; thus, pressure-induced changes in NMR parameters include the effect of mechanical compression of each conformer as well as a population shift among the conformers.

Structural Characteristics of the High-Energy Excited N_2 State. The high population of N_2 in Q41N allowed us to conduct a standard NMR structure calculation. The structure is of high quality and shows that the Q41N mutation leads to a weakened interaction between the loop and β_3-strand. Because the acceptor partner of the N41 side chain is not present within a reasonable hydrogen bonding distance (~3 Å), the hydrogen bond between the I36 C═O group and the Q41 side chain NH_2 protons, which is a highly conserved structural feature of the ubiquitin family of proteins, could be severely weakened or broken in Q41N (N_2 model). Although the structure and CLEANEX-PM analysis show that the N41 side chain exists in the protein interior and its side chain NH_2 group is protected from solvent as seen in the WT protein (see Figure S5A of the Supporting Information for WT and Figure S5B of the Supporting Information for Q41N), the weakened interaction in the mutant introduces further changes in interactions between α_1-helix and neighboring regions. Q41N has an increased amplitude of picosecond to nanosecond motion (e.g., 0° → 27°) of the NH group at the center of the helix. The amide hydrogens on residues 31−41 at the end of α_1-helix, the following loop, and β_3-strand of Q41N are rapidly exchanged with solvent protons, while they are much protected from exchange in the WT protein. These data indicate that the end of α_1-helix, the following loop and β_3-strand in Q41N have looser packing and their backbone amide groups are fully or partially hydrogen bonded with solvent water. The weaker atomic packing allows greater penetration of water into the protein interior. The increases in chain entropy and hydration entropy overcoming the losses of interactions would contribute to a stabilization of the N_2 conformer in the Q41N sample. The water penetration in N_2 gives N_2 a smaller partial molar volume than N_1, explaining why it is favored at high pressure. The effects of the K11A and E34A mutations were smaller than those of the Q41N and Q41A mutations, showing that the I36 C═O···Q41 Nε hydrogen bond is more important for the N_1−N_2 equilibrium than the K11−E34 salt bridge. Indeed, pH titration NMR experiments for Asp and Glu side chains showed that E34 was not involved in significant salt bridge interaction in WT protein (data not shown), although the side chains of K11 and E34 were found to form a surface-exposed salt bridge in the solution structure (PDB entry 1D3Z).

Water−Amide Proton Exchange and Thermodynamic Stability. Amide hydrogen atoms found in the backbone of folded proteins exchange protons with the solvent water at a slower rate than in unfolded proteins. Proteins in a native conformation have a strong tendency for the secondary structure to remain relatively protected from proton exchange. However, when the structure unfolds into an intermediate or unfolded forms, the amide hydrogens become more exposed to water and therefore exchange more quickly. In this CLEANEX-PM approach, it was observed that magnetization of protons is transferred from the solvent water to the amide groups during the mixing period of 0.005−0.1 s. This magnetization transfer is only observed among the amide groups that are exposed to the solvent water.

According to a previous high-pressure NMR study,[18] the transition rates k_{12} ($N_1 \rightarrow N_2$) and k_{21} ($N_2 \rightarrow N_1$) in the WT protein are estimated to be 0.72×10^5 and 4.1×10^5 s^{-1}, respectively, at 293 K and 30 bar. Therefore, under these experimental conditions (pH 7.2, 298 K, and 1 bar), k_{12} and k_{21}

dx.doi.org/10.1021/bi301420m | Biochemistry 2013, 52, 1874−1885

are much faster than the rate of exchange of amide hydrogens with solvent water in an unstructured peptide, k_{rc} ($10-10^3$ s^{-1}).[52] While conventional hydrogen−deuterium exchange NMR spectroscopy detects slower proton exchange with protection factors of $>10^3$ (17 kJ/mol at 298 K), this CLEANEX measurement detects rapid proton exchange that is scarcely observed in the hydrogen−deuterium exchange NMR measurement at neutral pH. The amide hydrogens on residues 31−41 in α_1-helix, the following loop, and β_3-strand of Q41N rapidly exchanged with protons, while they were protected from exchange in the WT protein. Indeed, the WT protein residues in the stable α_1-helix and β-sheet structures showed ΔG_{HX} values that had a much higher stability than 17 kJ/mol, even at low pH (pD* 3.5 and 295 K).[53] These data indicate that the ends of α_1-helix, the following loop, and the β_3-strand regions in Q41N have loose atomic packing and lower stability than the other regions. These structural and dynamic characteristics of Q41N coincide with those of N_2 of WT ubiquitin observed by high-pressure NMR and MD simulation, which suggests a swinging out of α_1-helix and the following loop and concomitant penetration of water into a hydrophobic core of the protein.[18]

Novel Recognition Dynamics of Ubiquitin. Ubiquitination leads to a wide range of functional consequences, including proteasomal degradation, DNA repair, cellular trafficking, immune responses, and chromatin remodeling.[54] In all these cases, ubiquitin is covalently attached to its target by the sequential activity of E1-activating, E2-conjugating, and E3-ligase enzymes. There are several other proteins that are attached to targets in analogous ways, such as NEDD8 and SUMO. This requires ubiquitin to interact with a wide range of proteins. In many cases, it interacts via a hydrophobic patch centered on I44 on β_5-strand, but other sites have also been identified, including an α/β groove between α_1-helix and β_2-strand and an "alternative site" centered on I36.[55,56] Structures of complexes bound at the hydrophobic patch show that ubiquitin adopts a range of conformations, which have been shown to sample the major conformational fluctuations of ubiquitin.[9] It is therefore important to ask whether the N_2 conformation is part of this fluctuation or is in other ways functionally relevant.

So far, microsecond time scale backbone motion at four particular residues (I23, N25, T55, and V70) in ubiquitin has been observed by NMR spin relaxation experiments.[25,28] The chemical exchange process at these residues was considered to result from disruption of N-cap hydrogen bonds of α_1-helix. Indeed, it has been demonstrated by X-ray crystallography that two conformations of ubiquitin that are similar in their overall folds but differ in these regions of the conformers can be identified.[27] This backbone dynamics observed at the residues seems to be a part of a native state ensemble of the protein rather than the N_1-N_2 fluctuation.

Several dynamic ensembles of ubiquitin have been described, in particular EROS,[9] ERNST,[57] and DER.[7] The EROS and ERNST structural ensembles are refined against NOEs and RDCs and therefore contain information about solution dynamics up to microseconds, while DER is refined against NOEs and order parameters, S^2; thus, the DER ensemble contains information about the dynamics on a picosecond to nanosecond time scale. A principal component analysis was conducted over all these ensemble conformations. A projection of the ensembles onto principal components 1 and 2 is shown in Figure S9 of the Supporting Information. Interestingly, the Q41N structures as well as the WT at 3 kbar cluster separately from the three ensembles, indicating that the N_1-N_2 fluctuation taking place on the 1−10 μs time scale is different from the native state dynamics taking place within microseconds.[7,9,57] Q41N is also different from the structure of the ubiquitin−Vps27 UIM complex, which is bound at the hydrophobic patch.[51,58] This implies that N_2 is not involved in the conformational change associated with the hydrophobic patch. In support of this conclusion, we note that the affinity of ubiquitin for the UIM was identical for WT and Q41N, and that the N_2 conformer was still significantly present in the UIM-bound mutant (Figure S8 of the Supporting Information). These results indicate that the N_1-N_2 fluctuation is orthogonal to binding at the hydrophobic patch and could be a novel recognition dynamics of ubiquitin that was previously inaccessible.

Several other binding sites have been identified on ubiquitin.[55] One of these is centered at I36, in the $\alpha_1-\beta_3$ loop, and is thus coincident with the N_1-N_2 conformational change. We previously found that the $\alpha_1-\beta_3$ loop of ubiquitin was involved in its conjugation onto the UbcH5b E2 enzyme.[56] There are now six structures in the Protein Data Bank of E2−ubiquitin conjugates.[57,59] SAXS and NMR found three different binding positions for the ubiquitin conjugation, "closed", "open", and "backbent". Although two structures utilize the canonical recognition surface of the $\beta_1-\beta_2$ turn and β_3-strand, in four of the structures, the interaction between ubiquitin and E2 is strikingly at the $\alpha_1-\beta_3$ loop (and at the C-terminus of ubiquitin, where E2 is attached), as shown in Figure S10 of the Supporting Information. The binding site of the $\alpha_1-\beta_3$ loop seems to be used when ubiquitin poses at the backbent position in E2−ubiquitin conjugates.[59] Just as interactions at the hydrophobic patch operate by conformational selection and select different conformers from the major ensembles, it seems likely that interactions in the $\alpha_1-\beta_3$ loop select different conformations here and at the $\beta_1-\beta_2$ turn. We therefore propose that N_2 represents a conformational change that is required during the E2 conjugation process. This functional role is consistent with the observation that similar high-energy states were conserved in a group of post-translational ubiquitin-like modifiers having the E1−E2−E3 interaction cascade, specifically NEDD8[19] and SUMO-2.[21]

CONCLUSION

Rational mutation based on the characteristics of the structure and dynamics of proteins obtained from pressure experiments is a new strategy for amplifying particular fluctuations in proteins. We have demonstrated that this approach leads to significant advances in the study of the structure and function of the marginally populated high-energy states of proteins. Multiple NMR analyses have demonstrated that the ubiquitin mutant Q41N is stable and preferentially adopts the N_2 conformation that has been characterized by high-pressure NMR spectroscopy[18] and MD simulation.[22] In this work, we present the high-resolution structure of the N_2 conformer at atmospheric pressure. We also show that a hydrogen bond between the I36 backbone carbonyl group and the Q41 side chain amide group is critical for controlling the N_1-N_2 dynamic motion of the protein. We suggest that N_1-N_2 fluctuation that is a novel recognition dynamics beyond the native state dynamics can be important for the events that occur during conjugation by the E2 enzyme. Considering that N_1-N_2 fluctuation is conserved in other post-translational

ubiquitin-like modifiers,[19] the Q41N mutant is useful for further structural and functional studies of ubiquitin and ubiquitin-related systems.

■ ASSOCIATED CONTENT

Supporting Information

Figures S1−S10. This material is available free of charge via the Internet at http://pubs.acs.org.

■ AUTHOR INFORMATION

Corresponding Author

*College of Pharmaceutical Sciences, Ritsumeikan University, 1-1-1 Noji-higashi, Kusatsu 525-8577, Japan. Telephone: +81-77-561-5751. Fax: +81-77-561-2659. E-mail: ryo@ph.ritsumei.ac.jp.

Funding

This work was supported by a Grant-in-Aid for Scientific Research on Innovative Areas from the MEXT of Japan to R.K., K.S., and K.K., a Grant-in-Aid for Young Scientists (B) from the MEXT of Japan to R.K., a Grant for Targeted Proteins Research Program from the Ministry of Education, Culture, Sports, Science and Technology to K.K., and a SUNBOR research grant to R.K. M.Y.-U. was a recipient of a Japan Society for the Promotion of Science Research Fellowship for Young Scientists.

Notes

The authors declare no competing financial interest.

■ ACKNOWLEDGMENTS

We thank Naohiro Kobayashi for instructions for KUJIRA, Takahisa Ikegami for instructions for RDC measurements, Hiroshi Imai for helping with peptide synthesis, Alana Simorellis for useful comments, and Hugh Dannatt for help with relaxation dispersion. We also thank RIKEN SSBC for NMR collaboration and providing KUJIRA and the Protein Research Institute of Osaka University for use of the AVANCE3-950 NMR spectrometer.

■ ABBREVIATIONS

RDC, residual dipolar coupling; rmsd, root-mean-square deviation; CLEANEX-PM, phase-modulated clean chemical exchange; HSQC, heteronuclear single-quantum coherence; NOE, nuclear Overhauser effect; PDB, Protein Data Bank.

■ REFERENCES

(1) Boehr, D. D., McElheny, D., Dyson, H. J., and Wright, P. E. (2006) The dynamic energy landscape of dihydrofolate reductase catalysis. *Science 313*, 1638−1642.

(2) Eisenmesser, E. Z., Millet, O., Labeikovsky, W., Korzhnev, D. M., Wolf-Watz, M., Bosco, D. A., Skalicky, J. J., Kay, L. E., and Kern, D. (2005) Intrinsic dynamics of an enzyme underlies catalysis. *Nature 438*, 117−121.

(3) Mulder, F. A., Mittermaier, A., Hon, B., Dahlquist, F. W., and Kay, L. E. (2001) Studying excited states of proteins by NMR spectroscopy. *Nat. Struct. Biol. 8*, 932−935.

(4) Sugase, K., Dyson, H. J., and Wright, P. E. (2007) Mechanism of coupled folding and binding of an intrinsically disordered protein. *Nature 447*, 1021−1025.

(5) Korzhnev, D. M., Religa, T. L., Banachewicz, W., Fersht, A. R., and Kay, L. E. (2010) A transient and low-populated protein-folding intermediate at atomic resolution. *Science 329*, 1312−1316.

(6) Tzeng, S. R., and Kalodimos, C. G. (2009) Dynamic activation of an allosteric regulatory protein. *Nature 462*, 368−372.

(7) Lindorff-Larsen, K., Best, R. B., DePristo, M. A., Dobson, C. M., and Vendruscolo, M. (2005) Simultaneous determination of protein structure and dynamics. *Nature 433*, 128−132.

(8) Meiler, J., Peti, W., and Griesinger, C. (2003) Dipolar couplings in multiple alignments suggest α helical motion in ubiquitin. *J. Am. Chem. Soc. 125*, 8072−8073.

(9) Lange, O. F., Lakomek, N. A., Farès, C., Schröder, G. F., Walter, K. F. A., Becker, S., Meiler, J., Grubmüller, H., Griesinger, C., and de Groot, B. L. (2008) Recognition dynamics up to microseconds revealed from an RDC-derived ubiquitin ensemble in solution. *Science 320*, 1471−1475.

(10) Bouvignies, G., Vallurupalli, P., Hansen, D. F., Correia, B. E., Lange, O., Bah, A., Vernon, R. M., Dahlquist, F. W., Baker, D., and Kay, L. E. (2011) Solution structure of a minor and transiently formed state of a T4 lysozyme mutant. *Nature 477*, 111−114.

(11) Neudecker, P., Robustelli, P., Cavalli, A., Walsh, P., Lundstrom, P., Zarrine-Afsar, A., Sharpe, S., Vendruscolo, M., and Kay, L. E. (2012) Structure of an intermediate state in protein folding and aggregation. *Science 336*, 362−366.

(12) Kamatari, Y., Kitahara, R., Yamada, H., Yokoyama, S., and Akasaka, K. (2004) High-pressure NMR spectroscopy for characterizing folding intermediates and denatured states of proteins. *Methods 34*, 133−143.

(13) Li, H., and Akasaka, K. (2006) Conformational fluctuations of proteins revealed by variable pressure NMR. *Biochim. Biophys. Acta 1764*, 331−345.

(14) Schlesinger, M., and Hershko, A. (1998) *The Ubiquitin System*, Cold Spring Harbor Laboratory Press, Plainview, NY.

(15) Ciechanover, A. J., and Maswucci, M. G. (2002) *The ubiquitin-proteasome proteolytic system*, World Scientific Publishing Co., Singapore.

(16) Kitahara, R., Yamada, H., and Akasaka, K. (2001) Two folded conformers of ubiquitin revealed by high-pressure NMR. *Biochemistry 40*, 13556−13563.

(17) Kitahara, R., and Akasaka, K. (2003) Close identity of a pressure-stabilized intermediate with a kinetic intermediate in protein folding. *Proc. Natl. Acad. Sci. U.S.A. 100*, 3167−3172.

(18) Kitahara, R., Yokoyama, S., and Akasaka, K. (2005) NMR snapshots of a fluctuating protein structure: Ubiquitin at 30 bar-3 kbar. *J. Mol. Biol. 347*, 277−285.

(19) Kitahara, R., Yamaguchi, Y., Sakata, E., Kasuya, T., Tanaka, K., Kato, K., Yokoyama, S., and Akasaka, K. (2006) Evolutionally conserved intermediates between ubiquitin and NEDD8. *J. Mol. Biol. 363*, 395−404.

(20) Kitahara, R., Okuno, A., Kato, M., Taniguchi, Y., Yokoyama, S., and Akasaka, K. (2006) Cold denaturation of ubiquitin at high pressure. *Magn. Reson. Chem.* No. MRC44 Spec. Issue, S108−S113.

(21) Kitahara, R., Zhao, C., Saito, K., Koshiba, S., Ioune, M., Kigawa, T., Yokoyama, S., and Akasaka, K. (2008) Basic folded and low-populated locally disordered conformers of SUMO-2 characterized by NMR spectroscopy at varying pressures. *Biochemistry 47*, 30−39.

(22) Imai, T., and Sugita, Y. (2010) Dynamic correlation between pressure-induced protein structural transition and water penetration. *J. Phys. Chem. B 114*, 2281−2286.

(23) Vijay-Kumar, S., Bugg, C. E., and Cook, W. J. (1987) Structure of ubiquitin refined at 1.8 Å resolution. *J. Mol. Biol. 194*, 531−544.

(24) Nucci, N. V., Pometun, M. S., and Wand, A. J. (2011) Mapping the hydration dynamics of ubiquitin. *J. Am. Chem. Soc. 133*, 12326−12329.

(25) Massi, F., Grey, M. J., and Palmer, A. G. (2005) Microsecond timescale backbone conformational dynamics in ubiquitin studied with NMR $R_{1\rho}$ relaxation experiments. *Protein Sci. 14*, 735−742.

(26) Salvi, N., Ulzega, S., Ferrage, F., and Bodenhausen, G. (2012) Time scales of slow motions in ubiquitin explored by heteronuclear double resonance. *J. Am. Chem. Soc. 134*, 2481−2484.

(27) Huang, K. Y., Amodeo, G. A., Tong, L. A., and McDermott, A. (2011) The structure of human ubiquitin in 2-methyl-2,4-pentanediol: A new conformational switch. *Protein Sci. 20*, 630−639.

(28) Sidhu, A., Surolia, A., Robertson, A. D., and Sundd, M. (2011) A hydrogen bond regulates slow motions in ubiquitin by modulating a β-turn flip. *J. Mol. Biol. 411*, 1037−1048.
(29) Kiel, C., and Serrano, L. (2006) The ubiquitin domain superfold: Structure-based sequence alignments and characterization of binding epitopes. *J. Mol. Biol. 355*, 821−844.
(30) Cavanagh, J., Fairbrother, W. J., Palmer, A. G., III, and Skelton, N. J. (1996) *Protein NMR Spectroscopy: Principle and Practice*, Academic Press, San Diego.
(31) Delaglio, F., Grzesiek, S., Vuister, G. W., Zhu, G., Pfeifer, J., and Bax, A. (1995) NMRpipe: A multidimensional spectral processing system based on Unix pipes. *J. Biomol. NMR 6*, 277−293.
(32) Johnson, B. A., and Blevins, R. A. (1994) Nmr View: A computer program for the visualization and analysis of NMR data. *J. Biomol. NMR 4*, 603−614.
(33) Kobayashi, N., Iwahara, J., Koshiba, S., Tomizawa, T., Tochio, N., Güntert, P., Kigawa, T., and Yokoyama, S. (2007) KUJIRA, a package of integrated modules for systematic and interactive analysis of NMR data directed to high-throughput NMR structure studies. *J. Biomol. NMR 39*, 31−52.
(34) Akasaka, K., and Yamada, H. (2001) On-line cell high-pressure nuclear magnetic resonance technique: Application to protein studies. *Methods Enzymol. 338*, 134−158.
(35) Peterson, R. W., Nucci, N. V., and Wand, A. J. (2011) Modification of encapsulation pressure of reverse micelles in liquid ethane. *J. Magn. Reson. 212*, 229−233.
(36) Herrmann, T., Güntert, P., and Wüthrich, K. (2002) Protein NMR structure determination with automated NOE assignment using the new software CANDID and the torsion angle dynamics algorithm DYANA. *J. Mol. Biol. 319*, 209−227.
(37) Ottiger, M., Delaglio, F., Marquardt, J. L., Tjandra, N., and Bax, A. (1998) Measurement of dipolar couplings for methylene and methyl sites in weakly oriented macromolecules and their use in structure determination. *J. Magn. Reson. 134*, 365−369.
(38) Shen, Y., Delaglio, F., Cornilescu, G., and Bax, A. (2009) TALOS plus: A hybrid method for predicting protein backbone torsion angles from NMR chemical shifts. *J. Biomol. NMR 44*, 213−223.
(39) Zweckstetter, M., and Bax, A. (2001) Characterization of molecular alignment in aqueous suspensions of Pf1 bacteriophage. *J. Biomol. NMR 20*, 365−377.
(40) Lindorff-Larsen, K., Piana, S., Palmo, K., Maragakis, P., Klepeis, J. L., Dror, R. O., and Shaw, D. E. (2010) Improved side-chain torsion potentials for the Amber ff99SB protein force field. *Proteins 78*, 1950−1958.
(41) Farrow, N. A., Muhandiram, R., Singer, A. U., Pascal, S. M., Kay, C. M., Gish, G., Shoelson, S. E., Pawson, T., Forman-Kay, J. D., and Kay, L. E. (1994) Backbone dynamics of a free and a phosphopeptide-complexed Src homology-2 domain studied by ^{15}N NMR relaxation. *Biochemistry 33*, 5984−6003.
(42) Mandel, A. M., Akke, M., and Palmer, A. G. (1995) Backbone dynamics of *Escherichia coli* ribonuclease HI: Correlations with structure and function in an active enzyme. *J. Mol. Biol. 246*, 144−163.
(43) Cole, R., and Loria, J. P. (2003) FAST-Modelfree: A program for rapid automated analysis of solution NMR spin-relaxation data. *J. Biomol. NMR 26*, 203−213.
(44) Long, J., Garner, T. P., Pandya, M. J., Craven, C. J., Chen, P., Shaw, B., Williamson, M. P., Layfield, R., and Searle, M. S. (2010) Dimerisation of the UBA domain of p62 inhibits ubiquitin binding and regulates NF-κB signalling. *J. Mol. Biol. 396*, 178−194.
(45) Hwang, T. L., van Zijl, P. C. M., and Mori, S. (1998) Accurate quantitation of water-amide proton exchange rates using the Phase-Modulated CLEAN chemical EXchange (CLEANEX-PM) approach with a Fast-HSQC (FHSQC) detection scheme. *J. Biomol. NMR 11*, 221−226.
(46) Wilton, D. J., Tunnicliffe, R. B., Kamatari, Y. O., Akasaka, K., and Williamson, M. P. (2008) Pressure-induced changes in the solution structure of the GB1 domain of protein G. *Proteins 71*, 1432−1440.
(47) Kamatari, Y. O., Yamada, H., Akasaka, K., Jones, J. A., Dobson, C. M., and Smith, L. J. (2001) Response of native and denatured hen lysozyme to high pressure studied by ^{15}N/^{1}H NMR spectroscopy. *Eur. J. Biochem. 268*, 1782−1793.
(48) Han, B., Liu, Y., Ginzinger, S. W., and Wishart, D. S. (2011) SHIFTX2: Significantly improved protein chemical shift prediction. *J. Biomol. NMR 50*, 43−57.
(49) Lipari, G., and Szabo, A. (1982) Model-free approach to the interpretation of Nuclear Magnetic Resonance relaxation in macromolecules. 1. Theory and range of validity. *J. Am. Chem. Soc. 104*, 4546−4559.
(50) Lipari, G., and Szabo, A. (1982) Model-free approach to the interpretation of nuclear magnetic resonance relaxation in macromolecules. 2. Analysis of experimental results. *J. Am. Chem. Soc. 104*, 4559−4570.
(51) Swanson, K. A., Kang, R. S., Stamenova, S. D., Hicke, L., and Radhakrishnan, I. (2003) Solution structure of Vps27 UIM-ubiquitin complex important for endosomal sorting and receptor down-regulation. *EMBO J. 22*, 4597−4606.
(52) Bai, Y. W., Milne, J. S., Mayne, L., and Englander, S. W. (1993) Primary structure effects on peptide group hydrogen exchange. *Proteins 17*, 75−86.
(53) Pan, Y. Q., and Briggs, M. S. (1992) Hydrogen exchange in native and alcohol forms of ubiquitin. *Biochemistry 31*, 11405−11412.
(54) Wickliffe, K., Williamson, A., Jin, L. Y., and Rape, M. (2009) The multiple layers of ubiquitin-dependent cell cycle control. *Chem. Rev. 109*, 1537−1548.
(55) Winget, J. M., and Mayor, T. (2010) The diversity of ubiquitin recognition: Hot spots and varied specificity. *Mol. Cell 38*, 627−635.
(56) Sakata, E., Satoh, T., Yamamoto, S., Yamaguchi, Y., Yagi-Utsumi, M., Kurimoto, E., Tanaka, K., Wakatsuki, S., and Kato, K. (2010) Crystal structure of UbcH5b−ubiquitin intermediate: Insight into the formation of the self-assembled E2∼Ub conjugates. *Structure 18*, 138−147.
(57) Fenwick, R. B., Esteban-Martin, S., Richter, B., Lee, D., Walter, K. F. A., Milovanovic, D., Becker, S., Lakomek, N. A., Griesinger, C., and Salvatella, X. (2011) Weak long-range correlated motions in a surface patch of ubiquitin involved in molecular recognition. *J. Am. Chem. Soc. 133*, 10336−10339.
(58) Sgourakis, N. G., Patel, M. M., Garcia, A. E., Makhatadze, G. I., and McCallum, S. A. (2010) Conformational dynamics and structural plasticity play critical roles in the ubiquitin recognition of a UIM domain. *J. Mol. Biol. 396*, 1128−1144.
(59) Page, R. C., Pruneda, J. N., Amick, J., Klevit, R. E., and Misra, S. (2012) Structural insights into the conformation and oligomerization of E2−ubiquitin conjugates. *Biochemistry 51*, 4175−4187.